COBEM 2023 27TH INTERNATIONAL CONGRESS OF MECHANICAL ENGENEERING

ABCM Brazilian Society of Mechanical Sciences and Engineering
27th ABCM International Congress of Mechanical Engineering
December 04-08, 2023, Florianópolis-SC, Brazil

COB-2023-0046
EVALUATION OF CONVERGENCE OF VORTEX PANEL METHOD FOR OBTAINING AERODYNAMIC COEFFICIENTS FOR NACA 0012 AIRFOIL

Bernardo Maia de Mello Alves
Victor Santoro Santiago
André Luiz Tenório Rezende
Department of Mechanical Engineering, IME - Military Engineering Institute, 22290-270, Rio de Janeiro, RJ, Brazil
bernardommalves@gmail.com, santoro@ime.eb.br, arezende@ime.eb.br

Abstract. *In this work a numerical model for solving viscous, incompressible two-dimensional flows is applied, in a transient regime, around NACA 0012 airfoil for obtaining aerodynamic coefficients. The numerical model implements the panels method together with the vortex method, where the body is discretized in a polygon of straight panels with linear vorticity distribution, while the vorticity field is discretized using Lamb vortices. The potential solution for the panel method is obtained considering the non-penetration boundary condition on the surface of the studied body. The radii of the nuclei of the nascent vortices are obtained through diffusion distance theory. Simulations are performed considering a fixed number of nascent vortices per panel, as well as a variable number of nascent vortices considering the variation of panel length. Additionally, convergence tests are performed by satisfying Kutta condition in the first iteration. Variations in the positions of discrete vortices in space are calculated by integrating in time, by the 2^{nd} order Adams-Bashforth method, the velocities for the convective motion are obtained by accounting the influence of all cloud vortices and also the influence of the panels. The diffusive motion is obtained through the random walk method. In order to accelerate calculations, adtative fast multipole expansion is used.*

Keywords: *panel method, vortex method, aerodynamics, random walk method*

1. INTRODUCTION

The objective of the present work is to apply the vortex panel method under several different configurations in order to modify the traditional vortex method, introducing, as a feature of originality, a parameter that states a variable number of nascents vortex per panel.

De Carvalho Silva (2005) utilizes vortex panel method to obtain the velocity field around an airfoil, as well as the aerodynamic coefficients, using a single nascent vortex per panel, for a Reynolds number of 1.7×10^6, while Pereira *et al.* (2004) ran simulations around an airfoil with Vortex Panel Method using Random Walk Method for simulating the diffusive motion of discrete vortices. Santiago (2008) performed extensive simulations over several bodies, including NACA 0012, using Vortex Panel Method combined with a variety of methods for obtaining loads and aerodynamic coefficients. Santiago (2008) also presents a method for calculating the amount of nascent vortices per panel in order to obtain convergence by solving the potential flow with combined with nascent vortices, satisfying both non penetration and no slip condition on the surface. Santiago (2008) also performed tests varying several parameters for the simulations. The method for obtaining the number of nascent vortices per panel is used in this paper in order to evaluate the convergence for several nascent vortices per panel.

Based on the results of the above mentioned papers, this work intends to study the gain in convergence when constant numbers of nascent vortices per panel are used, as well as a variable number or vortices per panel, since the length of panels vary significantly over its perimeter.

The algorithm presented byCarrier *et al.* (1988) for fast adaptive multipole expansion is used in the present work to perform the convective stage of the flow.

Finally, this paper studies the behavior of the flow simulation when different restriction condition are used to obtain a single solution for Laplace's Equation. These conditions are: Kutta's condition and conservation of circulation.

2. KUTTA CONDITION AND CONSERVATION OF CIRCULATION

Kutta condition, which is proposed based on observation, states that the sharp trailling of an airfoil is a stagnation point, implying that the flow around the upper surface of an airfoil is parallel to that around the lower surface. It is important to notice that Kutta condition does not apply to transient regime, when the conservation of circulation must be satisfied.

Beside that, this work intends to study the behavior of convergence when Kutta condition is used for obtaining the

solution for the potential flow, given that such condition is somewhat existent when permanent regime is achieved. In other words, it is an attempt to bring the flow, in the first iteration (potential flow), to a condition that is more similar to that expected when convergence is achieved.

In order to illustrate the potential flow under both conditions cited above, Figures 1 and 2 show the streamlines for an angle of attack of $25°$. A thorough methodology for solving the potential flow is given by Katz and Plotkin (2001).

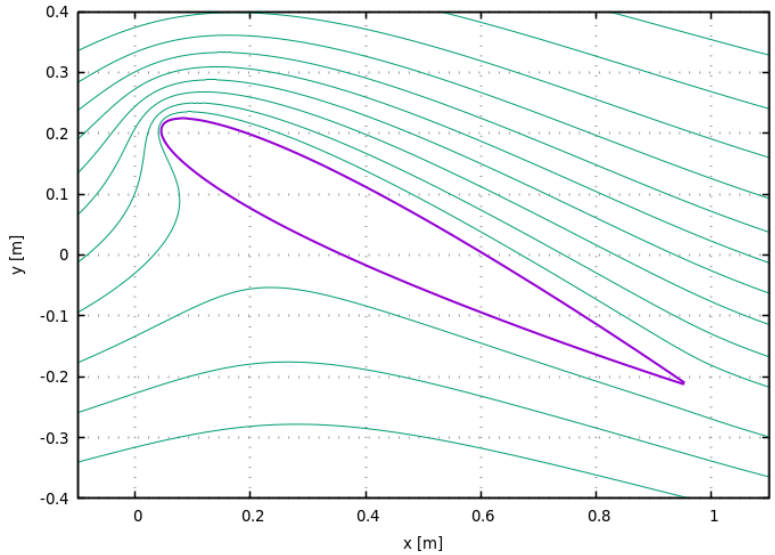

Figure 1. Streamlines for potential flow when Kutta condition is satisfied.

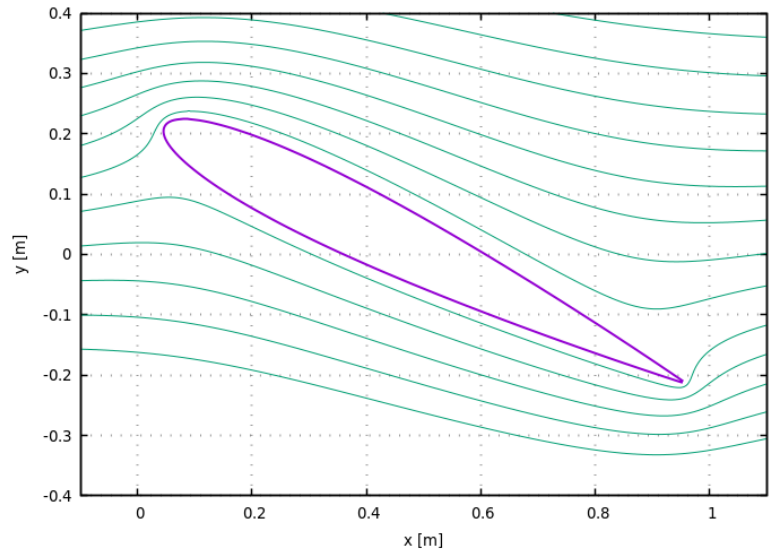

Figure 2. Streamlines for potential flow when conservation of circulation is satisfied.

2.1 Solution for the potential flow

The linear system of equations for obtaining the solutions showed in Figures 1 and 2, respectively, are shown below:

$$\begin{pmatrix} a_{11} & a_{12} & a_{13} & \dots & a_{1,N+1} \\ a_{21} & a_{22} & a_{23} & \dots & a_{2,N+1} \\ \dots & \dots & \dots & \dots & \dots \\ a_{N-1,1} & a_{N-1,2} & a_{N-1,3} & \dots & a_{N-1,N+1} \\ a_{N,1} & a_{N,2} & a_{N,3} & \dots & a_{N,N+1} \\ 1 & 0 & 0 & \dots & 1 \end{pmatrix} \begin{pmatrix} \gamma_1 \\ \gamma_2 \\ \dots \\ \gamma_{N-1} \\ \gamma_N \\ \gamma_{N+1} \end{pmatrix} = \begin{pmatrix} RHS_1 \\ RHS_2 \\ \dots \\ RHS_{N-1} \\ RHS_N \\ 0 \end{pmatrix} \tag{1}$$

$$\begin{pmatrix} a_{11} & a_{12} & ... & a_{1N} & a_{1,N+1} \\ a_{21} & a_{22} & ... & a_{2N} & a_{2,N+1} \\ ... & ... & ... & ... & ... \\ a_{N-1,1} & a_{N-1,2} & ... & a_{N-1,N} & a_{N-1,N+1} \\ a_{N,1} & a_{N,2} & ... & a_{N,N} & a_{N,N+1} \\ \Delta l_1/2 & (\Delta l_1 + \Delta l_2)/2 & ... & (\Delta l_{N-1} + \Delta l_N)/2 & \Delta l_N/2 \end{pmatrix} \begin{pmatrix} \gamma_1 \\ \gamma_2 \\ ... \\ \gamma_{N-1} \\ \gamma_N \\ \gamma_{N+1} \end{pmatrix} = \begin{pmatrix} RHS_1 \\ RHS_2 \\ ... \\ RHS_{N-1} \\ RHS_N \\ 0 \end{pmatrix} \tag{2}$$

Systems above are obtained when singularity elements are combined as solutions of Laplace's equation:

$$\nabla^2 \Phi(\mathbf{r}) = 0 \qquad \text{in flow domain} \tag{3a}$$

$$\nabla \Phi(\mathbf{r}) \cdot \mathbf{n} = \frac{\partial \Phi}{\partial \mathbf{n}} = 0 \qquad \text{on body surface} \tag{3b}$$

$$\lim_{\mathbf{r} \to \infty} |\nabla \Phi(\mathbf{r}, t)| = 1 \qquad \text{in farfield} \tag{3c}$$

Coefficients $a_{i,j}$ combined with the singularities γ_i are simply the Biot-Savart law for a given singularity element/distribution. Δl_i are the lengths of the panels. In this work, the linear vorticity distribution is used as singularity function. The right hand side (RHS) of the systems are the non penetration condition, namely Eq. 3b, while Eq. 3c is automatically satisfied by the decay characteristics of the singularity functions.

3. VISCOUS FLOW

The viscous flow is taken into account by using Navier-Stokes equation. Moreover, voticity is related to velocity by $\boldsymbol{\omega} = \nabla \times \mathbf{u}$. Vortex methods use the Vorticity Transport Equation, which is obtained by taking the curl of Navier-Stokes Equation (Batchelor (1967)):

$$\frac{D\boldsymbol{\omega}}{Dt} = \frac{\partial \boldsymbol{\omega}}{\partial t} + \mathbf{u} \cdot \nabla \boldsymbol{\omega} = \boldsymbol{\omega} \cdot \nabla \mathbf{u} + \frac{1}{Re} \nabla^2 \boldsymbol{\omega} \tag{4}$$

where

- $\partial \boldsymbol{\omega} / \partial t$ - local voriticty variation;
- $\mathbf{u} \cdot \nabla \boldsymbol{\omega}$ - vorticity convective transport;
- $\frac{1}{Re} \nabla^2 \boldsymbol{\omega}$ - vorticity diffusive transport; and
- $\boldsymbol{\omega} \cdot \nabla \mathbf{u}$ - deformation and stretching.

For the two dimensional case:

$$\frac{\partial \omega}{\partial t} + \mathbf{u} \cdot \nabla \omega = \frac{1}{Re} \nabla^2 \omega \tag{5}$$

Vortex method requires convective and diffusive phase to be solved separately. Thus, for the convective phase we have

$$\frac{\partial \omega}{\partial t} + \mathbf{u} \cdot \nabla \omega = 0 \tag{6}$$

and for the diffusive phase we have

$$\frac{\partial \omega}{\partial t} = \frac{1}{Re} \nabla^2 \omega \tag{7}$$

3.1 Convective motion

Convective motion derives from the velocity induced in the particles by the free flow, by the body (discretized singularities) and by the free vortices in the viscous wake:

$$\begin{pmatrix} u \\ v \end{pmatrix}_i = \begin{pmatrix} u_b \\ v_b \end{pmatrix}_i + \begin{pmatrix} u_v \\ v_v \end{pmatrix}_i + \begin{pmatrix} u_\infty \\ v_\infty \end{pmatrix}_i \tag{8}$$

The velocity induced by the free flow is simply $u_\infty = V_\infty cos(\alpha)$ and $v_\infty = V_\infty sin(\alpha)$.

For a body discretized in linear vortex distribution panels, Biot-Savart law consists of

$$u_j^p = \frac{y}{2\pi}\left(\frac{\gamma_{j+1}-\gamma_j}{x_{j+1}-x_j}\right) ln\left(\frac{r_{j+1}}{r_j}\right) + \frac{\gamma_1(x_{j+1}-x_j)+(\gamma_{j+1}-\gamma_j)(x-x_j)}{2\pi(x_{j+1}-x_j)}(\theta_{j+1}-\theta_j) \tag{9}$$

$$v_j^p = -\frac{\gamma_1(x_{j+1}-x_j)+(\gamma_{j+1}-\gamma_j)(x-x_j)}{2\pi(x_{j+1}-x_j)} ln\left(\frac{r_j}{r_{j+1}}\right) + \frac{y}{2\pi}\left(\frac{\gamma_{j+1}-\gamma_j}{x_{j+1}-x_j}\right)\left[\frac{x_{j+1}-x_j}{y} + (\theta_{j+1}-\theta_j)\right] \tag{10}$$

where u^p and v^p are the velocities in the panel coordinate system. To convert such velocities into the global coordinate system, we have

$$\begin{pmatrix} u_j \\ v_j \end{pmatrix} = \begin{pmatrix} cos(\beta_i) & sen(\beta_i) \\ -sen(\beta_i) & cos(\beta_i) \end{pmatrix} \begin{pmatrix} u_j^p \\ v_j^p \end{pmatrix} \tag{11}$$

where β is the panel orientation angle as shown in Figure 3 shown below

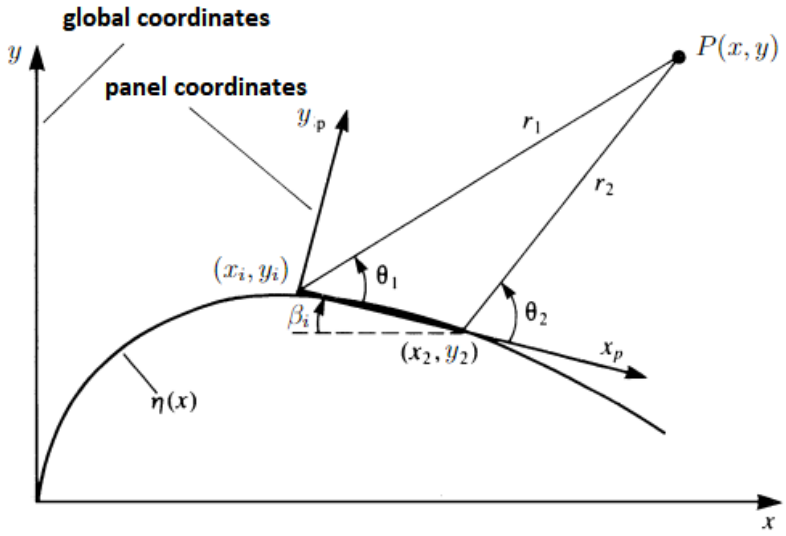

Figure 3. Panel coordinate system (source: adapted from Katz and Plotkin, 2001).

The discrete vortex in the present work are modeled as a Lamb-Vortex, and the velocities induced by the such vortices are

$$\begin{pmatrix} u_v \\ v_v \end{pmatrix}_i = \sum_{j=1}^{M} \begin{pmatrix} \frac{\Gamma_j}{2\pi}\frac{y-y_0}{r^2}\left[1-exp\left(-\frac{r^2}{\sigma_0^2}\right)\right] \\ -\frac{\Gamma_j}{2\pi}\frac{x-x_0}{r^2}\left[1-exp\left(-\frac{r^2}{\sigma_0^2}\right)\right] \end{pmatrix} \tag{12}$$

$$r = (x-x_0)^2 + (y-y_0)^2$$

where Γ is the vorticity and σ_0 is the nuclei radii. In order to obtain convective displacement, Eq. 8 is integrated in time using Adams-Basforth method.

3.2 Diffusive motion

Diffusive motion is obtained by solving Eq. 7, which gives

$$\omega(r,t) = Re\frac{\Gamma}{4\pi t} exp\left(-Re\frac{r^2}{4t}\right) \tag{13}$$

Eq. 13 can be modeled as a Brownian motion, such methodology consisting of the Random Walk Method, as shown by Chorin (1973) and Lewis (1991), which gives

$$\Delta r = \sqrt{\frac{4t}{Re} ln\left(\frac{1}{P}\right)} \tag{14a}$$

$$\Delta\theta = 2\pi Q \tag{14b}$$

$$\begin{pmatrix}\Delta x_D \\ \Delta y_D\end{pmatrix}_i = \begin{pmatrix}\Delta r\ cos(\Delta\theta) \\ \Delta r\ sen(\Delta\theta)\end{pmatrix} \tag{15}$$

where P and Q are random numbers between 0 and 1.

3.3 Vortices generation

By using continuity equation and substituting on 7, we have

$$\frac{\partial\omega}{\partial t} = \nu\frac{\partial^2\omega}{\partial y^2} \tag{16a}$$

$$\nu\frac{\partial\omega}{\partial y}(x, y = 0, t > 0) = \frac{-\gamma(x)}{\delta t} \tag{16b}$$

$$\omega(x, y \to \infty, t > 0) = 0 \tag{16c}$$

$$\omega(x, y > 0, t = 0) = 0 \tag{16d}$$

By solving the equation above by similarity, de Carvalho Silva (2005) gives that the diffusion distance is

$$\delta_n = k_s\frac{\delta_t}{\sqrt{Re}} \tag{17}$$

Pereira *et al.* (2004), de Carvalho Silva (2005), Santiago (2008) and other authors state that a suitable value for δ_t for convergence is $0.01 \leq \delta_t \leq 0.05$. For the purpose of this paper, a value of $\delta_t = 0.025$ will be used, and Eq. 17 becomes

$$\delta_n = \frac{k}{\sqrt{Re}} \tag{18}$$

where k encompasses k_s and δ_t and is adjusted for a given simulation. Cabrera (1998) and de Carvalho Silva (2005) performed simulations using 1 nascent discrete vortex per panel, resulting in a poorly dense vortex cloud which reflects in the method convergence, as the coefficients fluctuate over time in a somewhat sinusoidal shape. Therefore, a statistical treatment is need for obtaining a value for the coefficients under investigation.

Santiago (2008) presents a method for simulating various nascent vortices per panel in order to increase convergence, eliminating the numerical fluctuations cited above, at the cost of enhanced computation time. Santiago (2008) states the number of vortices per painel for convergence is obtained as (further development is omitted here)

$$L = \left[\frac{2\pi^2}{8}\frac{Re}{N}\frac{1}{\left(h/\sigma_0\right)^4}\right]^{1/3} \tag{19}$$

In Eq. 19, N is the number of panels and it is assumed that the length of a panel is $N/2$, and h/σ_0 is the overlay ratio, as shown in Figure 4.

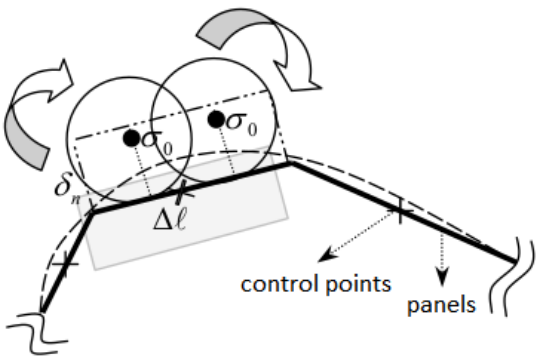

Figure 4. Vortex generation on the surface of the body based on diffusion distance.

However, the length of panels will vary along its perimeter when full cosine method is used to discretize the airfoil geometry in order to refine the discretization on the leading and trailing edges. Figure 5 shows the variation for the panel

lengths of NACA 0012 when it is discretized in 180 panels. The lengths are normalized with respect to the smallest panel. In fact, Figure 5 shows us that the biggest panel has about 57 times the length of the smallest panel.

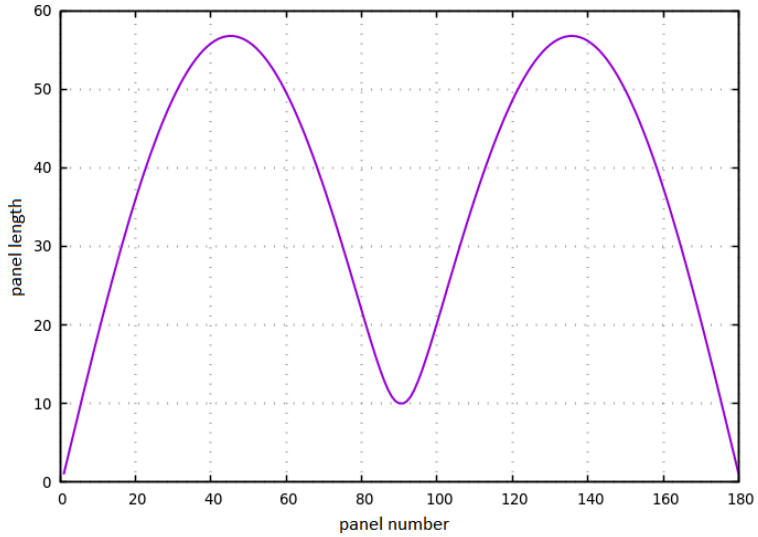

Figure 5. Panel length variation along its perimeter for NACA 0012 with180 panels.

In this sense, introducing the originality feature, this work intends to explore the behavior of convergence when such discrepancy in the panel lengths is taken into account. To achieve that, Eq. 19 is slightly modified as

$$L_i = \left[\frac{2\pi^2}{4}\frac{Re}{\Delta L_i}\frac{1}{\left(h/\sigma_0\right)^4}\right]^{1/3} \tag{20}$$

3.4 Discrete vortex radii

As presented by Cabrera (1998) and de Carvalho Silva (2005), the discrete vortex radius is equal to the diffusion distance illustrated in Figure 4:

$$\sigma_0 = \delta_n \tag{21}$$

$$\tag{22}$$

and the velocity induced by a discrete lamb vortex with a nucleus radii of σ_0 is

$$u(r) = -\frac{\Gamma}{2\pi r}\left[1 - exp\left(-5.02572.\frac{r^2}{\sigma_0^2}\right)\right] \tag{23}$$

By using equations 19 through 23, a series of simulations were performed in order to investigate the behavior of vortex panel methods for a variety of conditions, namely

- 1 nascent vortex per panel;
- 4 nascent vortices per panel;
- 10 nascent vortices per panel;
- L nascent vortices per panel, where L is determined by Eq. 19.
- L_i nascent vortices per panel, whereL_i is determined by Eq. 20.

4. RESULTS

Simulations mentioned above were performed using Kutta condition and conservation of circulation, resulting in a total of 24 simulations. All simulations shown in this section were performed using NACA 0012 airfoil discretized in 250 panels, diffusion distance and vortex radii $\sigma_0 = \delta_n = 0.005$, $\delta t = 0.025\ s$ and an overlay ratio of $h/\sigma_0 = 0.8$.

4.1 Simulation using Vorticity Conservation Law in the first iteration

Typical vortex clouds are shown in Figs. 6 to 9.

Figure 6. Vortex cloud for $Re = 1.7 \times 10^5$ and $\alpha = 6°$.

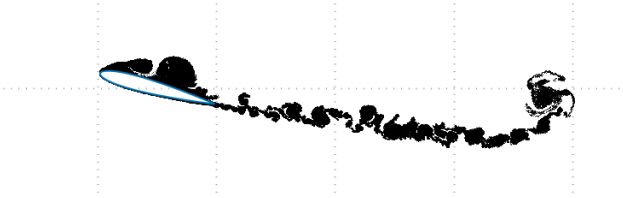

Figure 7. Vortex cloud for $Re = 1.7 \times 10^5$ and $\alpha = 15°$.

Figure 8. Vortex cloud for $Re = 1.0 \times 10^6$ and $\alpha = 6°$.

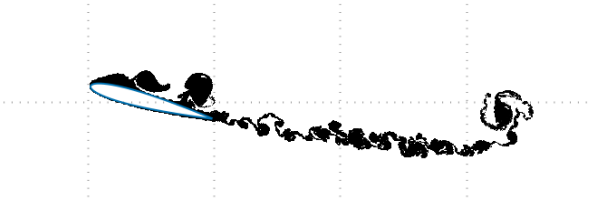

Figure 9. Vortex cloud for $Re = 1.0 \times 10^6$ and $\alpha = 15°$.

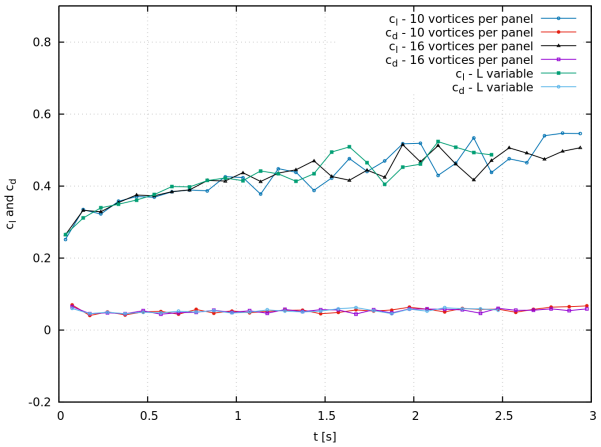

Figure 10. Convergence of C_l and C_d for $Re = 1.7 \times 10^5$ and $\alpha = 6°$.

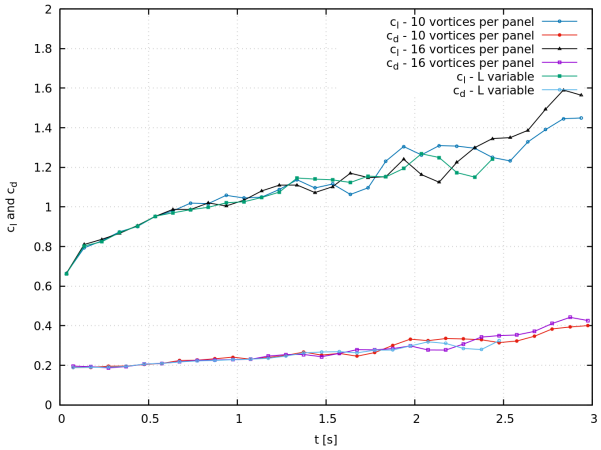

Figure 11. Convergence of C_l and C_d for $Re = 1.7 \times 10^5$ and $\alpha = 15°$.

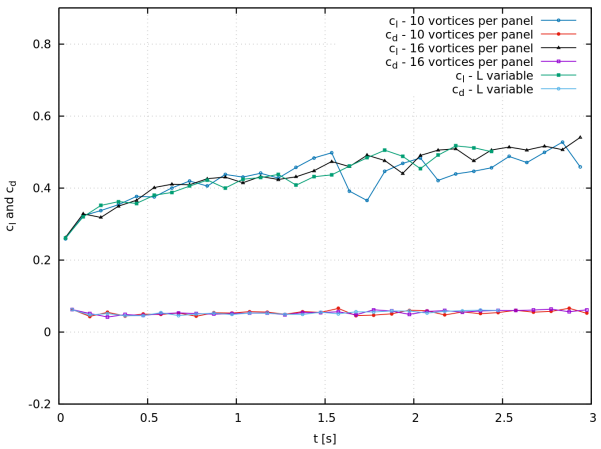

Figure 12. Convergence of C_l and C_d for $Re = 1.0 \times 10^6$ and $\alpha = 6°$.

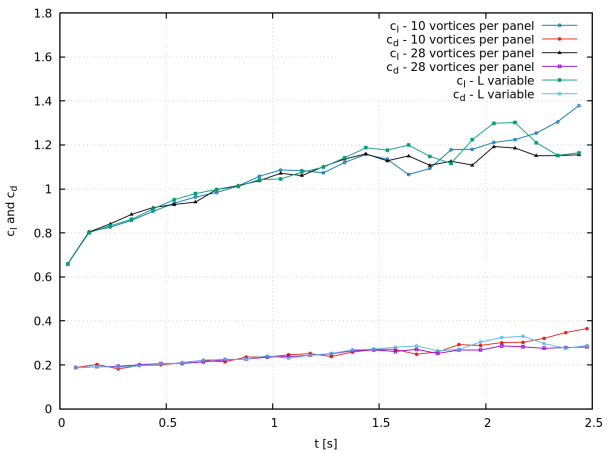

Figure 13. Convergence of C_l and C_d for $Re = 1.0 \times 10^6$ and $\alpha = 15°$.

4.2 Simulation using Kutta's Condition in the first iteration

Typical vortex clouds are shown in Figs. 14 to 17.

Figure 14. Vortex cloud for $Re = 1.7 \times 10^5$ and $\alpha = 6°$.

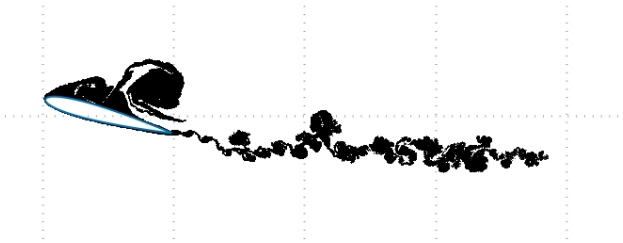

Figure 15. Vortex cloud for $Re = 1.7 \times 10^5$ and $\alpha = 15°$.

Figure 16. Vortex cloud for $Re = 1.0 \times 10^6$ and $\alpha = 6°$.

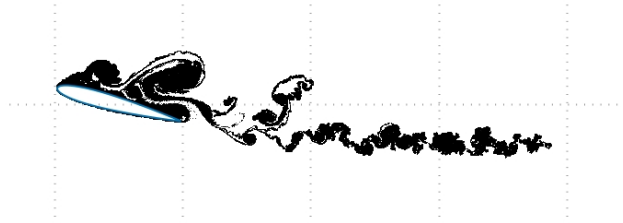

Figure 17. Vortex cloud for $Re = 1.0 \times 10^6$ and $\alpha = 15°$.

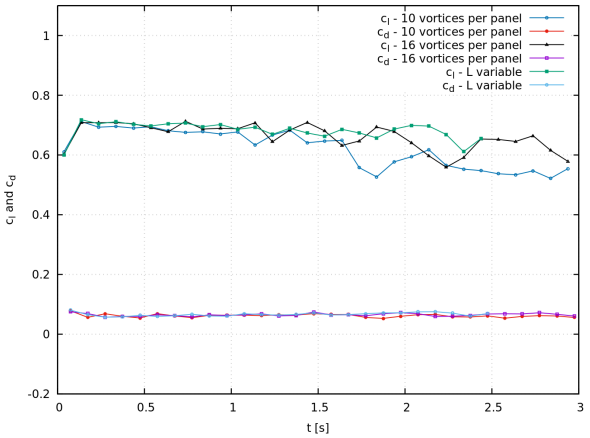

Figure 18. Convergence of C_l and C_d for $Re = 1.7 \times 10^5$ and $\alpha = 6°$.

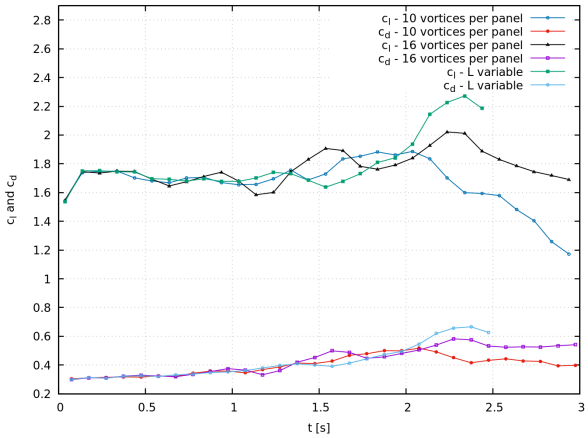

Figure 19. Convergence of C_l and C_d for $Re = 1.7 \times 10^5$ and $\alpha = 15°$.

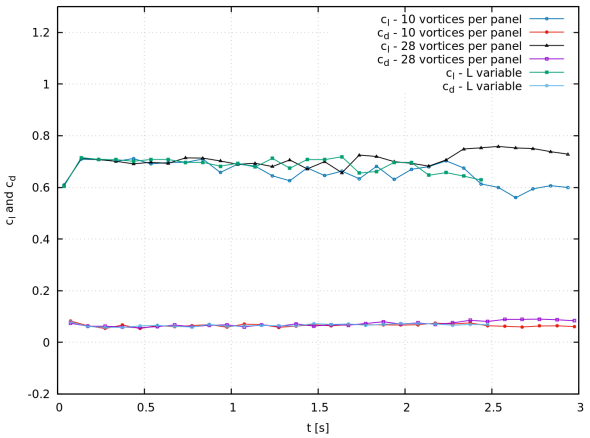

Figure 20. Convergence of C_l and C_d for $Re = 1.0 \times 10^6$ and $\alpha = 6°$.

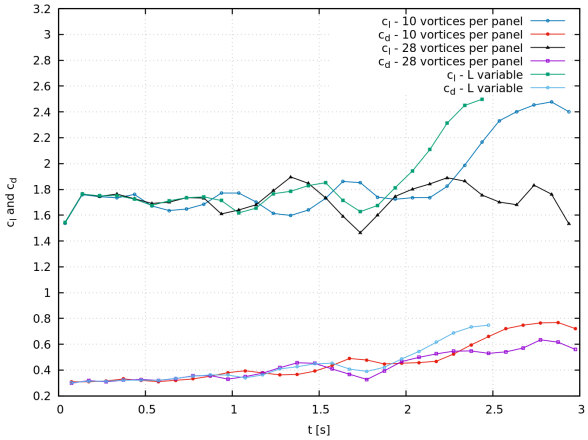

Figure 21. Convergence of C_l and C_d for $Re = 1.0 \times 10^6$ and $\alpha = 15°$.

5. FINAL DISCUSSION AND VALIDATION

A graphical analysis in Figs 10 to 13 shows that convergence is achieved earlier when a variable number of vortices is used. For example, in Figure 10 C_l has converged after $1.7\ s$ for a variable number of panels (obtained using Eq.20), while it converges after $2.5\ s$ when using 16 vortices per panel (obtained using Eq. 19).

The same trend is observed in Figs 18 to 21. It should be noticed, however, that the number of nascent vortices when constant vortices per panel are used is bigger than the other case. In other words, Eq. 20 will result in less nascent vortices than Eq. 19 due to truncation. Finally, it is necessary to analyze if earlier convergence actually results in less computation time. This can be achieved by analyzing the computation time curves. This will be done here for the case cited above (Fig 10).

For the first case, where $L = 16$, we have 4000 nascent vortices and convergence is achieved around $t = 2.5\ s$, which means 100 iterations were necessary ($t/\delta t = 2.5/0.025 = 100$). Thus, the simulation has converged when there are around 4.0×10^5 vortices in the cloud. For the second case, where L is variable, we have 3770 nascent vortices and convergence is achieved around $t = 1.7\ s$, which means 68 iterations were necessary, resulting in a vortex cloud composed of about 2.6×10^5. The computation time required can be obtained from Figure 22 below:

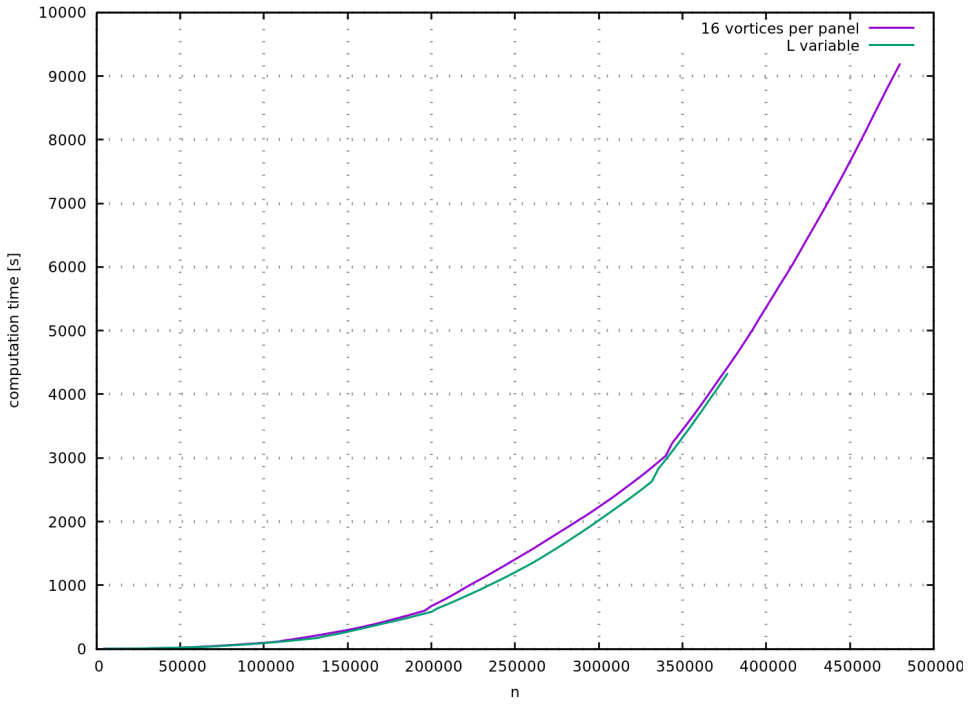

Figure 22. Computation time required for simulating NACA0012 with 250 panels, $Re = 1.7 \times 10^5$ and $\alpha = 6°$.

From the graphic shown above, it can be observed that the computation time required for convergence when a variable number of nascent vortices per panel is used was about $1600\ s$, while when a constant number of $L = 16$ vortices per panel is used the computation time required was about $5400\ s$.

No gain was observed when Kutta's condition was used in the first iteration. In fact, the use of such artifice has delayed convergence, although better results were obtained for the cases where viscous effects are less relevant (low angle of attack and high Reynolds number).

Lastly, to provide validation, a comparison of the model presented in this paper with other authors is shown in Figures 23 and 24. Blevins (1984) results were obtained experimentally and Spalart (2000) applies finite volumes method with turbulence model, while Pereira *et al.* (2004) and Santiago (2008) applied vortex panel method in order to obtain the results shown in the figure.

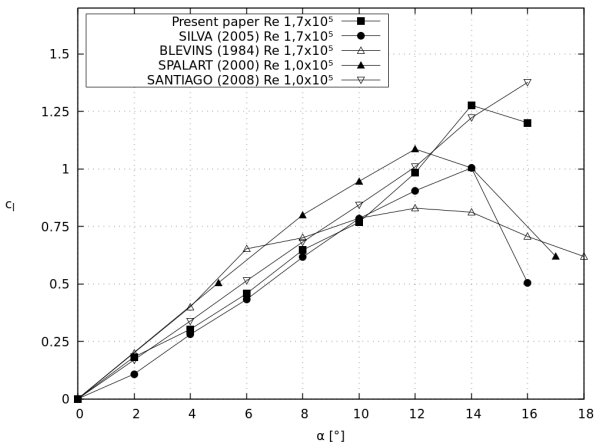

Figure 23. Variation of c_l with α by various authors.

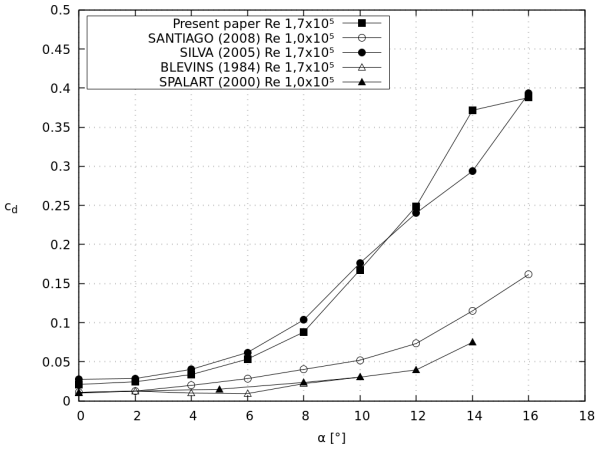

Figure 24. Variation of c_d with α by various authors.

As can be seen from the figure above, the results obtained with the present method are consistent with other found in the literature.

6. REFERENCES

Batchelor, G.K., 1967. *An Introduction to Fluid Dynamics*. Cambridge University Press, Cambridge, 1st edition.

Blevins, R.D., 1984. *Applied Fluid Dynamics Handbook*. Van Nostrand Reinhold, 1st edition.

Cabrera, A.A.M., 1998. *Simulação numérica do escoamento em torno de um cilindro circular e sem torção utilizando o método de vórtices discretos*. Dissertação de mestrado, Universidade Federal do Rio de Janeiro.

Carrier, J., Greengard, L. and Rokhlin, V., 1988. "A fast adaptive multipole algorithm for particle simulations". *Society for Industrial and Applied Mathematics*.

Chorin, A.J., 1973. "Numerial study of slightly viscous flow". *Journal of Fluid Mechanics*, Vol. 57, pp. 785–796.

de Carvalho Silva, D.F., 2005. *Simulação numérica do escoamento ao redor de aerofólios via método de vórtices associado ao método dos painéis*. Dissertação de mestrado, Universidade Federal do Rio de Janeiro.

Katz, J. and Plotkin, A., 2001. *Low-Speed Aerodynamics*. Cambridge University Press, Cambridge, 2nd edition.

Lewis, R.I., 1991. *Vortex Element Methods for Fluid Dynamic Analysis of Engineering Systems*. Cambridge University Press, Cambridge.

Pereira, L.H.G., Silva, D.F.C. and Bodstein, G.C.R., 2004. "Estudo numérico do escoamento potencial em torno de um aerofólio utilizando o método dos painéis". *ENCIT – 10° Congresso Brasileiro de Ciências Térmicas, Rio de Janeiro, RJ, Brasil*.

Santiago, V.S., 2008. *Modelagem numérica do escoamento ao redor de corpos aerodinâmicos utilizando o método de vórtices*. Universidade Federal do Rio de Janeiro, Rio de Janeiro.

Spalart, P.R., 2000. "Strategies for turbulence modelling and simulation". *International Journal of Heat and Fluid Flow*, Vol. 21, p 252-263.

7. RESPONSIBILITY NOTICE

The authors are solely responsible for the printed material included in this paper.